TEMPERATURE PROFILES OF ACCRETION DISKS AROUND RAPIDLY ROTATING NEUTRON STARS IN GENERAL RELATIVITY AND THE IMPLICATIONS FOR CYGNUS X-2

SUDIP BHATTACHARYYA[1] AND ARUN V. THAMPAN[2]

Indian Institute of Astrophysics, Koramangala, Bangalore 560 034, India

RANJEEV MISRA[3]

Inter-University Centre for Astronomy and Astrophysics, Post Bag 4, Ganeshkhind, Pune 411 007, India

AND

BHASKAR DATTA[4,5]

Indian Institute of Astrophysics, Koramangala, Bangalore 560 034, India

ABSTRACT

We calculate the temperature profiles of (thin) accretion disks around rapidly rotating neutron stars (with low surface magnetic fields), taking into account the full effects of general relativity. We then consider a model for the spectrum of the X-ray emission from the disk that is parameterized by the mass accretion rate, the color temperature, and the rotation rate of the neutron star. We derive constraints on these parameters for the X-ray source Cygnus X-2 using the estimates of the maximum temperature in the disk along with the disk and boundary layer luminosities, using the spectrum inferred from the *EXOSAT* data. Our calculations suggest that the neutron star in Cygnus X-2 rotates close to the centrifugal mass-shed limit. Possible constraints on the neutron star equation of state are also discussed.

Subject headings: accretion, accretion disks — stars: individual (Cygnus X-2) — stars: neutron — stars: rotation — X-rays: stars

1. INTRODUCTION

The soft X-ray spectra of luminous low-mass X-ray binaries (LMXBs) are believed to originate in the geometrically thin accretion disks around neutron stars with weak surface magnetic fields (see, e.g., White 1995). An important parameter in modeling these spectra is the maximum value of the effective temperature in the accretion disk. The effective temperature profile in the disk can be estimated (assuming that the disk radiates from its surface like a blackbody) if one knows the accretion energy released in the disk. In a Newtonian treatment, the innermost region of an accretion disk surrounding a neutron star with a weak magnetic field will extend rather close to the neutron star surface. The amount of energy released in the disk will be one-half of the total accretion energy, the other half being released in the thin boundary layer between the disk inner edge and the neutron star's surface. This then gives the disk an effective temperature T_{eff} that varies with the radial distance r as $T_{\text{eff}} \propto r^{-3/4}$, and the maximum effective temperature $T_{\text{eff}}^{\text{max}}$ will depend on the (nonrotating) neutron star mass M and the radius R as $T_{\text{eff}}^{\text{max}} \propto (M\dot{M}/R^3)^{1/4}$, where $\dot{M}$ is the steady state mass accretion rate. In this approach, the value of $T_{\text{eff}}^{\text{max}}$ in the disk occurs at a radial distance of 1.36 R.

Mitsuda et al. (1984) parameterized the disk spectrum by the maximum temperature of the disk using the above formalism and assumed that the mass of the neutron star is equal to 1.4 $M_\odot$. These authors assumed that the inner parts of the disk did not contribute to the X-ray spectrum and suggested a multicolor spectrum for the X-ray emission from the disk. It was shown by these authors that the observed spectra of Sco X-1, 1608−52, GX 349+2, and GX 5-1, obtained with the *Tenma* satellite, can be well-fitted with the sum of a multicolor spectrum and a single blackbody spectrum (presumably coming from the boundary layer). White, Stella, & Parmar (1988) (WSP) suggested that the simple blackbody accretion disk model should be modified to take into account the effects of electron scattering. Using *EXOSAT* observations, these authors compared the spectral properties of the persistent emission from a number of X-ray burst sources with various X-ray emission models. Their work suggests that either the neutron star (in each system considered) rotates close to equilibrium with the Keplerian disk or that most of the boundary layer emission is not represented by a blackbody spectrum.

For accretion disks around compact objects, one possibility is that the accretion disk is not Keplerian in nature. For example, Titarchuk, Lapidus, & Muslimov (1998) have formulated a boundary problem in which the Keplerian accretion flow in the inner disk is smoothly adjusted to the neutron star rotation rate. The generality of such a formulation permits application even to black holes but only for certain assumed inner boundary conditions. These authors demonstrate that there exists a transition layer (having an extent of the order of the neutron star radius) in which the accretion flow is sub-Keplerian. An attractive feature of this formalism is that it allows super-Keplerian motion at the outer boundary of the transition layer, permitting the formation of a hot blob that ultimately bounces out to the magnetosphere. This formalism (Osherovich & Titarchuk 1999a, 1999b; Titarchuk & Osherovich 1999; Titarchuk, Osherovich, & Kuznetsov 1999) therefore provides a mechanism for the production of high-frequency quasi-periodic oscillations (QPOs) observed in the X-ray flux

[1] Joint Astronomy Program, Indian Institute of Science, Bangalore 560 012, India; sudip@iiap.ernet.in; sudip@physics.iisc.ernet.in.

[2] Present Address: Inter-University Centre for Astronomy and Astrophysics (IUCAA), Pune 411 007, India; arun@iucaa.ernet.in.

[3] Present Address: Department of Physics and Astronomy, Northwestern University, 2131 Sheridan Road, Evanston, IL 60208-2900; ranjeev@yawara.astro.nwu.edu.

[4] Raman Research Institute, Bangalore 560 080, India.

[5] Deceased: 1999 December 3.

from several LMXBs. Such effects, when taken into account, can modify the Newtonian disk temperature profile (Chakrabarti & Titarchuk 1995).

There are several other effects that will modify the Newtonian disk temperature profile, such as the effects of general relativity and of irradiation of the disk by the central neutron star. The wind mass loss from the disk and the residual magnetic field near the disk inner edge may also play a part in modifying the effective temperature (Knigge 1999). Czerny, Czerny, & Grindlay (1986) calculated the LMXB disk spectra assuming that a disk radiates locally as a blackbody with the energy flux determined by viscous forces as well as irradiation by the boundary layer and took into account relativistic effects, some of them in an approximate way. The possible effects of general relativity were also discussed by Hanawa (1989), using the Schwarzschild (nonrotating) metric and assuming that the neutron star radius is less than the radius of the innermost stable circular orbit ($r_{in} = 6\,GM/c^2$), which he identified as the disk inner boundary. The color temperature was assumed to be higher than the effective temperature by a factor of 1.5. It was found by Hanawa (1989) that the observations are consistent with a geometrically thin, optically thick accretion disk whose inner edge is at $r = r_{in}$, with r being the Schwarzschild radial coordinate.

An important dynamical aspect of disk accretion onto a weakly magnetized neutron star is that the neutron star will get spun up to its equilibrium period, which is of the order of milliseconds (see Bhattacharya & van den Heuvel 1991 and references therein). The effect of rotation is to increase the equatorial radius of the neutron star and also to relocate the innermost stable circular orbit (for a corotating disk) closer to the stellar surface (as compared to the Schwarzschild case). These effects will be substantial for rapid rotation rates in a fully general relativistic treatment that includes rotation. Therefore, for accreting neutron stars with low magnetic fields, the stellar radius can be greater or less than the radius of the innermost stable orbit, depending on the neutron star equation of state (EOS) and on the spacetime geometry. The effect of the magnetic field will be to constrain the location of the inner edge of the accretion disk to the magnetospheric (Alfvén) radius. In such a case, r_{in} would lose the astrophysical relevance that is discussed here. However, this will be so only if the magnetic field strength B is large. The problem addressed in this paper refers to LMXBs that contain old neutron stars that are believed to have undergone sufficient magnetic field decay (Bhattacharya & Datta 1996). Clearly, for low magnetic field case, a number of different disk geometries will be possible if the general relativistic effects of rotation are taken into account. These structural differences influence the effective temperature profile, and the conclusions derived by Czerny et al. (1986) and Hanawa (1989) are likely to be modified.

In this paper we attempt to highlight the effects of general relativity and the rotation of the neutron star on the accretion disk temperature profile and then apply them to the particular case of the X-ray source Cygnus X-2. For simplicity, we (unlike Titarchuk et al. 1998) assume the accretion disk to be fully Keplerian, geometrically thin, and optically thick. We first give a theoretical estimate of the modifications in T_{col}^{max} that would result if the inclusion of the rotational effects of general relativity were made and illustrate these modifications by taking representative neutron

star EOSs. We then consider a model for the spectrum parameterized by the mass accretion rate, the color factor, and the rotation rate of the accreting neutron star (assumed to be weakly magnetized). We derive constraints on these parameters for the X-ray source Cygnus X-2, for which we take the estimates of T_{eff}^{max}, the disk luminosity, and the boundary layer luminosity from the analysis of WSP. A conclusion of our work is that the neutron star in Cygnus X-2 has a rapid spin rate close to the centrifugal mass-shed limit.

The format of this paper is as follows: In § 2 we discuss the rotational general relativistic effects on the disk temperature using a formalism given by Page & Thorne (1974), and we also discuss the disk irradiation by the neutron star. The theoretical predictions for the temperature profiles with these effects taken into account are presented in § 3. Section 4 deals with the comparison of observations and its implications for the parameters of our model for Cygnus X-2. A summary and discussions are presented in § 5.

2. THE EFFECTIVE TEMPERATURE OF THE DISK

2.1. Effects of General Relativity and Rotation

The effective temperature in the disk (assumed to be optically thick) is given by

$$T_{eff} = (F/\sigma)^{1/4} , \tag{1}$$

where σ is the Stephan-Boltzmann constant and F is the X-ray energy flux per surface area. We use the formalism given by Page & Thorne (1974), who gave the following general relativistic expression for F emitted from the surface of an (geometrically thin and non–self-gravitating) accretion disk around a rotating black hole:

$$F(r) = \frac{\dot{M}}{4\pi r} f(r) , \tag{2}$$

where

$$f(r) = -\Omega_{K,r}(\tilde{E} - \Omega_K \tilde{l})^{-2} \int_{r_{in}}^{r} (\tilde{E} - \Omega_K \tilde{l})\tilde{l}_{,r} dr . \tag{3}$$

Here r_{in} is the disk inner edge radius, $\tilde{E}$ and $\tilde{l}$ are the specific energy and the specific angular momentum of a test particle in a Keplerian orbit, and Ω_K is the Keplerian angular velocity at radial distance r. In our notation, a comma followed by a variable as subscript to a quantity represents a derivative of the quantity with respect to the variable. Also, in this paper, we use the geometric units $c = G = 1$.

For accreting neutron stars located within the disk's inner edge, the situation is analogous to the black hole binary case, and the above formula, using a metric describing a rotating neutron star, can be applied directly for our purpose. However, unlike the black hole binary case, there can be situations for neutron star binaries where the neutron star radius exceeds the innermost stable circular orbit radius. In such situations the boundary condition, assumed by Page & Thorne (1974), that the torque vanishes at the disk inner edge, will not be strictly valid. The use of equation (1) will then be an approximation. This will affect the temperatures close to the disk inner edge but not T_{eff}^{max} to any significant degree (see § 5 for discussion).

In order to evaluate T_{eff} using equation (1), we need to know the radial profiles of $\tilde{E}$, $\tilde{l}$, and Ω_K. For this, we first have to compute the equilibrium sequences of neutron stars in rapid rotation. These can be calculated by noting that the

spacetime around a rotating neutron star can be described by the following metric (Cook, Shapiro, & Teukolsky 1994):

$$ds^2 = g_{\lambda\beta} dx^\lambda dx^\beta \quad (\lambda, \beta = 0, 1, 2, 3)$$
$$= -e^{\gamma+\rho} dt^2 + e^{2\alpha}(d\bar{r}^2 + \bar{r}^2 d\theta^2)$$
$$+ e^{\gamma-\rho}\bar{r}^2 \sin^2 \theta(d\phi - \omega dt)^2 , \qquad (4)$$

where the metric potentials γ, ρ, α, and the angular velocity (ω) of local inertial frame with respect to an observer at infinity are all functions of the quasi-isotropic radial coordinate ($\bar{r}$) and the polar angle (θ); $\bar{r}$ is related to the Schwarzschild radial coordinate (r) through the equation $r = \bar{r}e^{(\gamma-\rho)/2}$.

On the assumptions that the matter is a perfect fluid and that the spacetime described by metric (4) is stationary, axisymmetric, asymptotically flat, and reflection-symmetric (about the equatorial plane), the Einstein field equations reduce to three nonhomogeneous, second-order, coupled differential equations (for γ, ρ, and ω) and one ordinary differential equation (for α) in terms of ϵ and P (the total energy density and the pressure of neutron star matter, respectively) in addition to terms involving γ, ρ, ω, and α (see Komatsu, Eriguchi, & Hachisu 1989). We have solved these equations (self-consistently and numerically) to obtain γ, ρ, ω, α, P, and Ω (which is the angular velocity of the neutron star matter as measured by a distant observer) as functions of $\bar{r}$ and θ. The angular velocity enters into the equations through the rotation law (which must be specified) for the matter distribution. The equilibrium solutions so obtained can then be used to calculate bulk structure parameters such as gravitational mass M, equatorial radius R, angular momentum J, etc., of the rotating neutron star. We assume that the neutron star rotates rigidly. Thus, Ω is constant for the stellar matter distribution and is taken to be equal to Ω_*, where Ω_* is defined as the angular velocity of the neutron star as measured by a distant observer.

Equation (1) gives the effective disk temperature $T_{\rm eff}$ with respect to an observer comoving with the disk. From the observational viewpoint, this temperature must be modified, taking into account the gravitational redshift and the rotational Doppler effect. In order to keep our analysis tractable, we use the expression given in Hanawa (1989) for this modification:

$$1 + z = \left(1 - \frac{3M}{r}\right)^{-1/2} . \qquad (5)$$

With this correction for $1 + z$, we define a temperature relevant for observations ($T_{\rm obs}$) as

$$T_{\rm obs} = \frac{1}{1 + z} T_{\rm eff} . \qquad (6)$$

2.2. Computation of $\tilde{E}$, $\tilde{l}$, and Ω_K

For the work presented in this paper, we compute constant gravitational mass (M) equilibrium sequences for rigidly and rapidly rotating neutron stars using the formalism described above (see Datta, Thampan, & Bombaci 1998 for details), keeping in mind the importance of the parameters M and Ω_* for modeling the X-ray emission from LMXBs. These sequences are constructed starting from the static limit all the way up to the rotation rate corresponding to the centrifugal mass-shed limit. The latter limit corresponds to the maximum Ω_* ($= \Omega_{\rm ms}$) for which centrifugal forces are able to balance the inward gravitational force. We

now briefly describe how the quantities $\tilde{E}$, $\tilde{l}$, and Ω_K are calculated; for details, the reader is referred to Thampan & Datta (1998). For a material particle in the gravitational field described by metric (4), we can write down the equation of motion in the equatorial plane (see, e.g., Misner, Thorne, & Wheeler 1973). These will be in terms of $\tilde{E}$, $\tilde{l}$, ω, $\bar{r}$, and the metric coefficients. The equation of motion in the radial direction defines the effective gravitational potential. The two conditions for orbits (circularity and extremum) at any r yield values for $\tilde{E}$ and $\tilde{l}$ as given by

$$\tilde{E} - \omega\tilde{l} = \frac{e^{(\gamma+\rho)/2}}{\sqrt{1 - v^2}} , \qquad (7)$$

$$\tilde{l} = \frac{v\bar{r}e^{(\gamma-\rho)/2}}{\sqrt{1 - v^2}} , \qquad (8)$$

where $v = (\Omega - \omega)\bar{r}e^{-\rho} \sin \theta$ is the physical velocity of the matter. The equations of motion in the azimuthal direction and in the time direction yield the Keplerian angular velocity:

$$\Omega_K = e^{2\rho(\bar{r})} \frac{\tilde{l}/\bar{r}^2}{(\tilde{E} - \omega\tilde{l})} + \omega(\bar{r}) . \qquad (9)$$

2.3. Computation of $E_{\rm BL}$ and E_D

We define the specific gravitational energy release due to the ingress of a material particle from infinity to the disk inner edge as E_D, and that due to the particle spiraling in from the disk inner edge to the surface of the star as the boundary layer energy $E_{\rm BL}$. For the case where the disk inner edge coincides with the stellar surface, $E_{\rm BL}$ is the difference in the energy of the particle in a Keplerian orbit at $r = R$ and that when it is at rest on the stellar surface. The exact expressions for $E_{\rm BL}$ and E_D are determined by the effective potential corresponding to any given spacetime metric. For the Schwarzschild metric and the "slow"-rotation Hartle-Thorne metric, the boundary layer–to–disk luminosity ratio has been calculated by Sunyaev & Shakura (1986) and Datta, Thampan, & Wiita (1995), respectively. Calculations of $E_{\rm BL}$ and E_D corresponding to the metric (4) and used for the modeling in this paper are discussed in detail in Thampan & Datta (1998).

2.4. Disk Irradiation by the Neutron Star

For luminous LMXBs, there can be substantial irradiation of the disk surface by the radiation coming from the neutron star boundary layer. The radiation temperature at the surface of a disk irradiated by a central source is given by (King, Kolb, & Burderi 1996)

$$T_{\rm irr}(r) = \left[\frac{\eta\dot{M}c^2(1 - \beta)}{4\pi\sigma r^2} \frac{h}{r} (n - 1)\right]^{1/4} , \qquad (10)$$

where η is the efficiency of conversion of accreted rest mass to energy, β is the X-ray albedo, h is the half-thickness of the disk at r, and n is given by the relation $h \propto r^n$. For the actual values of β, h/r, and n needed for our computation here, we choose the same values (i.e., 0.9, 0.2, and 9/7, respectively) as given in King et al. (1996). Although the above equation is derived based on Newtonian considerations, corrections due to general relativity (including that of rapid rotation) will be manifested through the factor η. We have made a

general relativistic evaluation of η for various neutron star rotating configurations, corresponding to realistic neutron star EOS models, as described in Thampan & Datta (1998). Since $T_{irr}(r) \propto r^{-1/2}$ and $T_{eff}(r) \propto r^{-3/4}$, T_{irr} will dominate over T_{eff} only at large distances. The net effective temperature of the disk will be given by (see Vrtilek et al. 1990)

$$T_{disk}(r) = [T_{eff}^4(r) + T_{irr}^4(r)]^{1/4} . \qquad (11)$$

For the Cygnus X-2 modeling presented here, we find that T_{irr} does not play any significant role. However, since this quantity has consequences for the disk instability, we calculate it using equation (10) and illustrate it for the rotating neutron star models considered here.

3. RESULTS FOR THE DISK TEMPERATURE PROFILE

3.1. Neutron Star Equations of State

The neutron star EOS is an important determining factor for the structure parameters of the star. A variety of neutron star EOSs is available in the literature, ranging from very soft to very stiff models. For the purpose of our calculation, we have chosen four EOS models: (A) Pandharipande (1971) (hyperons), (B) Baldo, Bombaci, & Burgio (1997) (AV14 + 3bf), (C) Walecka (1974), and (D) Sahu, Basu, & Datta (1993). Of these, model A is soft, model B is intermediate in stiffness, and models C and D are stiff EOS. With this representative choice of EOS, the results of our calculations are expected to be of sufficient generality.

3.2. The Results

We have calculated the disk temperature profiles for rapidly rotating, constant gravitational mass sequences of neutron stars in general relativity. For our purpose here, we choose two values for the gravitational mass, namely, 1.4

$M_\odot$ and 1.78 $M_\odot$, the former being the canonical mass for neutron stars (as inferred from binary X-ray pulsar data), while the latter is the estimated mass for the neutron star in Cygnus X-2 (Orosz & Kuulkers 1999). It may be noted with caution (Haberl & Titarchuk 1995) that this value is not confirmed from X-ray burst spectral analysis. We use the value of $M = 1.78\ M_\odot$ for the illustration of our results and leave the issue for future confirmation. In order to make a comparison with observations of Cygnus X-2, we need to calculate the values of the E_{BL}, E_D, and T_{eff}^{max} as functions of the stellar rotation rate Ω_* for the above chosen values of the gravitational mass (M).

In Table 1 we list the values of the stellar rotation rate at centrifugal mass shed limit Ω_{ms}; the neutron star radius R; the radius of the inner edge of the disk r_{in}; E_{BL}, E_D, and the ratio E_{BL}/E_D; T_{eff}^{max} and T_{obs}^{max} and r_{eff}^{max} and r_{obs}^{max} for the two mentioned values of M and for the different EOS models. The last nine computed quantities are given for two values of neutron star rotation rate, namely, the static limit ($\Omega_* = 0$) and the centrifugal mass shed limit ($\Omega_* = \Omega_{ms}$). The quantities E_D and E_{BL} are in specific units (i.e., units of rest energy $m_0 c^2$ of the accreted particle). The temperatures are expressed in units of $\dot{M}_{17}^{1/4} \times 10^5$ K (where $\dot{M}_{17} = \dot{M}/10^{17}$ g s^{-1}). From this table it may be seen that for a given neutron star, gravitational mass (M): (1) Ω_{ms} decreases for increasing stiffness of the EOS model. (2) The radius R is greater for stiffer EOSs. (3) The behavior of r_{in} depends on whether $r_{ms} > R$ or $r_{ms} < R$ and hence appears nonmonotonic. (4) The energy E_{BL} for the nonrotating configuration decreases with the stiffness of the EOS. For a configuration rotating at the mass shed limit, E_{BL} is insignificant. (5) In the nonrotating limit, E_D remains roughly constant for the varying stiffness of the EOS model. However, for the rapidly rotating case, the value of E_D

TABLE 1
THEORETICALLY COMPUTED PARAMETERS

PARAMETER	Ω	MODEL A 1.4 $M_\odot$	MODEL B 1.4 $M_\odot$	MODEL B 1.78 $M_\odot$	MODEL C 1.4 $M_\odot$	MODEL C 1.78 $M_\odot$	MODEL D 1.4 $M_\odot$	MODEL D 1.78 $M_\odot$
Ω_{ms} (10^3 rad s^{-1}).........		11.026	7.001	8.219	6.085	6.808	4.652	5.088
R (km)......................	$\Omega = 0$	7.46	11.01	9.84	12.28	12.32	14.74	15.76
	$\Omega = \Omega_{ms}$	11.44	15.72	15.19	17.26	17.28	20.74	21.16
r_{in} (km).....................	$\Omega = 0$	12.40	12.41	15.81	12.41	15.75	14.74	15.79
	$\Omega = \Omega_{ms}$	11.44	15.72	15.19	17.26	17.28	20.74	21.16
E_{BL} ($m_0\ c^2$).................	$\Omega = 0$	0.275	0.153	0.262	0.128	0.185	0.097	0.136
	$\Omega = \Omega_{ms}$	9.0 E-5	5.0 E-5	5.0 E-5	4.0 E-5	1.4 E-4	1.4 E-4	6.0 E-5
E_D ($m_0\ c^2$).................	$\Omega = 0$	0.057	0.057	0.057	0.057	0.057	0.055	0.057
	$\Omega = \Omega_{ms}$	0.073	0.057	0.071	0.053	0.064	0.045	0.054
E_{BL}/E_D	$\Omega = 0$	4.809	2.673	4.574	2.248	3.239	1.779	2.387
	$\Omega = \Omega_{ms}$	1.0 E-3	9.0 E-4	7.0 E-4	8.0 E-4	2.0 E-3	3.0 E-3	1.0 E-3
T_{eff}^{max} ($\dot{M}_{17}^{1/4} \times 10^5$ K)......	$\Omega = 0$	47.64	47.64	42.16	47.64	42.16	45.98	42.16
	$\Omega = \Omega_{ms}$	56.94	46.54	49.28	43.80	45.45	38.32	39.42
r_{eff}^{max} (km)	$\Omega = 0$	19.76	19.76	25.18	19.75	25.06	21.13	25.16
	$\Omega = \Omega_{ms}$	16.14	21.64	21.42	23.68	24.05	28.39	29.21
T_{obs}^{max} ($\dot{M}_{17}^{1/4} \times 10^5$ K)......	$\Omega = 0$	39.98	39.98	35.05	39.98	35.05	38.87	35.05
	$\Omega = \Omega_{ms}$	45.99	39.98	39.98	37.79	37.79	33.95	33.95
r_{obs}^{max} (km)	$\Omega = 0$	22.29	22.31	28.45	22.31	28.30	23.44	28.41
	$\Omega = \Omega_{ms}$	18.70	23.69	24.58	25.60	26.90	30.14	31.72

NOTE.—Centrifugal mass shed limit (Ω_{ms}), the neutron star radius (R), the disk inner edge radius (r_{in}), the specific gravitational energy release in the boundary layer (E_{BL}) and in the disk (E_D), their ratio (E_{BL}/E_D), the maximum effective temperature (T_{eff}^{max}), the radial location (r_{eff}^{max}) in the disk corresponding to T_{eff}^{max} and T_{obs}^{max} (see text), and the radial location (r_{obs}^{max}) corresponding to this. These values are listed for two values of M for all of the EOS models considered here (except for EOS model [A], where the maximum neutron star mass is less than 1.78 $M_\odot$, so only $M = 1.4\ M_\odot$ is considered). The number following the letter E represents powers of 10.
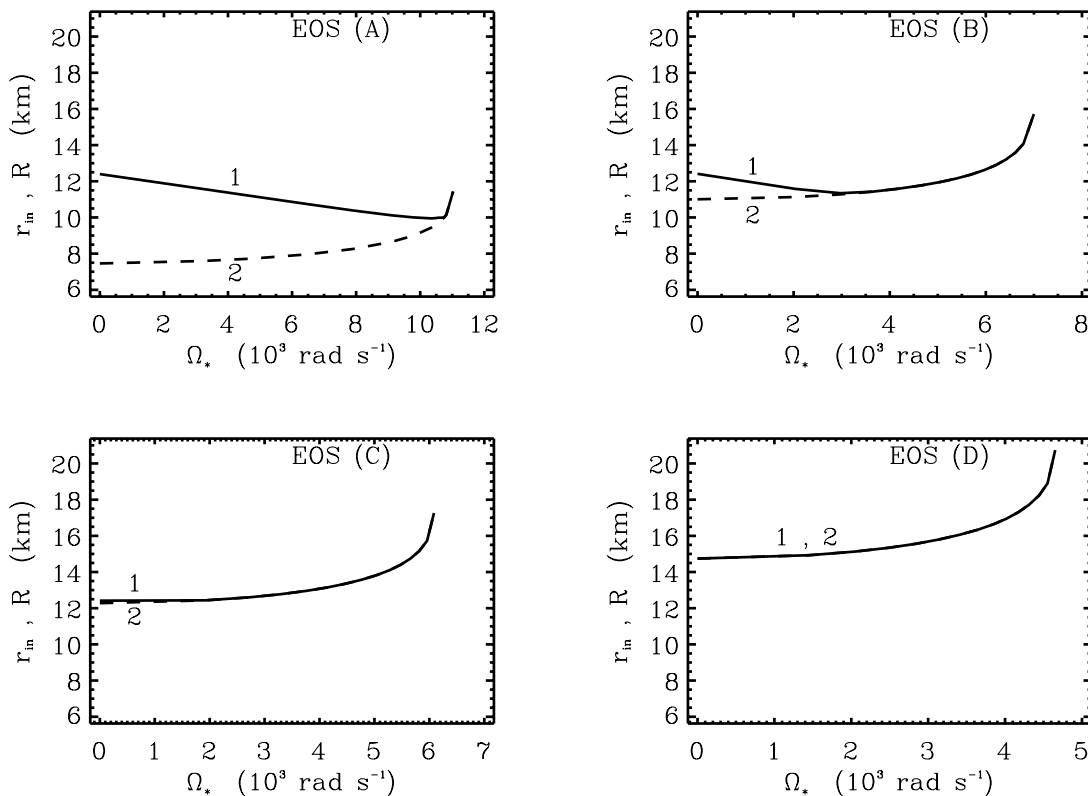
FIG. 1.—Disk inner edge radius (r_{in}; *curve 1*) and neutron star radius (R; *curve 2*) as functions of the neutron star angular velocity (Ω_*) for various EOS models. The curves are for a fixed gravitational mass ($M = 1.4\,M_\odot$) of the neutron star.

decreases with increasing stiffness. (6) The ratio E_{BL}/E_D in static limit is highest for the softest EOS model. For the rapidly rotating case, this ratio is uniformly insignificant. (7) The temperatures T_{eff}^{max} and T_{obs}^{max} decrease with increasing stiffness of the EOS models. However, these values exhibit nonmonotonic variation with Ω_* (see Fig. 5 for the first parameter). (8) The rest of the parameters, namely, r_{eff}^{max} and r_{obs}^{max}, are nonmonotonic with respect to the EOS stiffness parameter.

In Figure 1 we display the variation of R (*dashed curve*) and r_{in} (*continuous curve*) with Ω_* for $M = 1.4\,M_\odot$ for the four EOS models that we have chosen. From this figure it is seen that for a constant gravitational mass sequence, and for both soft and intermediate EOS models, $r_{in} > R$ for slow rotation rates, whereas for rapid rotation rates $r_{in} = R$. In other words, for neutron stars spinning very rapidly, the inner edge of the disk will almost coincide with the stellar surface. It may be noted that for the stiff EOS models, this condition obtains even at slow rotation rates of the neutron star.

It is instructive to make a comparison between the temperature profiles calculated using a Newtonian prescription with that obtained in a relativistic description using the Schwarzschild metric. This is shown in Figure 2 for the EOS model B and $M = 1.4\,M_\odot$ (the trend is similar for all the EOS models). The vertical axis in this figure is T_{eff} (in this and all other figures except Fig. 6 the temperatures are shown in units of $\dot{M}_{17}^{1/4} \times 10^5$ K), and in the horizontal axis the radial distance is in kilometers. This figure underlines the importance of general relativity in determining the accretion disk temperature profiles; the Schwarzschild result for T_{eff}^{max} is always less than the Newtonian result, and, for

the neutron star configuration considered here, the overestimate is almost 25%. For the sake of illustration, we also show the corresponding curve for a neutron star rotating at the mass shed limit (*curve 4*, Fig. 5). The disk inner edge is at the radius of the innermost stable circular orbit for all the cases. Note that the disk inner edge should be at R for
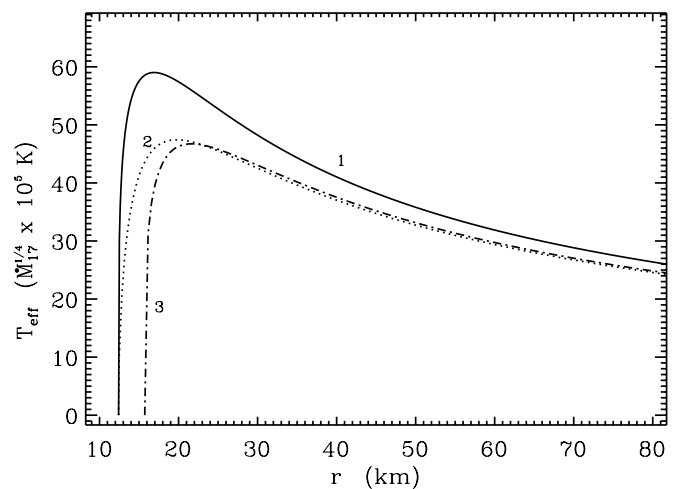
FIG. 2.—General relativistic corrections to the Newtonian temperature profiles for EOS model B and the neutron star gravitational mass $M = 1.4\,M_\odot$. Curve 1 corresponds to the Newtonian case, curve 2 to the Schwarzschild case, and curve 3 to a neutron star rotating at the centrifugal mass shed limit, calculated using the metric (4). For curve 1, it is assumed that $r_{in} = 6GM/c^2$. In this and all subsequent figures (except Fig. 6) the temperature is expressed in units of $\dot{M}_{17}^{1/4}\,10^5$ K, where $\dot{M}_{17}$ is the steady state mass accretion rate in units of 10^{17} g s^{-1}.
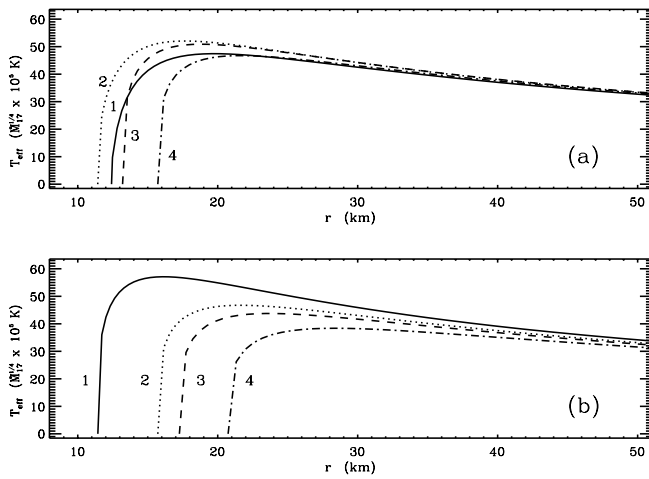
FIG. 3.—Temperature profiles incorporating the effects of rotation of the neutron star. The plots correspond to (a) EOS model B and an assumed neutron star mass of $M = 1.4\,M_\odot$ for rotation rates $\Omega_* = 0$ (*curve 1*), $\Omega_* = 3.647 \times 10^3$ rad s^{-1} (*curve 2*), $\Omega_* = 6.420 \times 10^3$ rad s^{-1} (*curve 3*), and $\Omega_* = 7.001 \times 10^3$ rad s$^{-1} = \Omega_{ms}$ (*curve 4*), and (b) the same assumed mass and $\Omega_* = \Omega_{ms}$ for the EOS models A (*curve 1*), B (*curve 2*), C (*curve 3*), and D (*curve 4*).

Newtonian case, but we have taken $r_{in} = 6GM/c^2$ as assumed in Shapiro & Teukolsky (1983).

The effect of neutron star rotation on the accretion disk temperature, treated generally relativistically, is illustrated in Figures 3a and 3b. Figure 3a corresponds to the EOS model B. The qualitative features of this graph are similar for the other EOS models and are not shown here.

However, the temperature profiles exhibit a marked dependence on the EOS. This dependence is illustrated in Figure 3b, which is done for a particular value of $\Omega_* = \Omega_{ms}$. All these temperature profiles have been calculated for a neutron star mass equal to 1.4 $M_\odot$. The temperature profiles shown in Figure 3a do not have a monotonic behavior with respect to Ω_*. This behavior is a composite of two underlying effects: (1) the energy flux emitted from the disk increases with Ω_* and (2) the nature of the dependence of r_{in} (where T_{eff} vanishes, i.e., the boundary condition) on Ω_* (see Fig. 1). This is more clearly brought out in Figure 4, where we have plotted T_{eff} versus Ω_* for selected constant radial distances (indicated in six different panels) and EOS (B). At large radial distances the value T_{eff} is almost independent of the boundary condition; hence the temperature always increases with Ω_* in Figure 4f.

The variations of E_D, E_{BL}, the ratio E_{BL}/E_D, and T_{eff}^{max} with Ω_* are displayed in Figure 5 for all EOS models considered here. All the plots correspond to $M = 1.4\ M_\odot$. Unlike the constant central density neutron star sequences (Thampan & Datta 1998), for the constant gravitational mass sequences E_D does not have a general monotonic behavior with Ω_*. The quantity T_{eff}^{max} has a behavior akin to that of E_D (because of the reasons mentioned earlier). The energy E_{BL} decreases with Ω_*, slowly at first but rapidly as Ω_* tends to Ω_{ms}. The variation of E_{BL}/E_D with respect to Ω_* is similar to that of E_{BL}.

In Figure 6 we provide a comparison between the effective temperature (eq. [1]) and the irradiation temperature (eq. [10]) profiles (both in units of $\dot{M}_{17}^{1/4}$ K). We have taken $\eta = E_{BL} + E_D$. Figure 6a is for $\Omega_* = 0$, while Figure 6b is for a higher $\Omega_* = 6420$ rad s^{-1}. The curves are for the
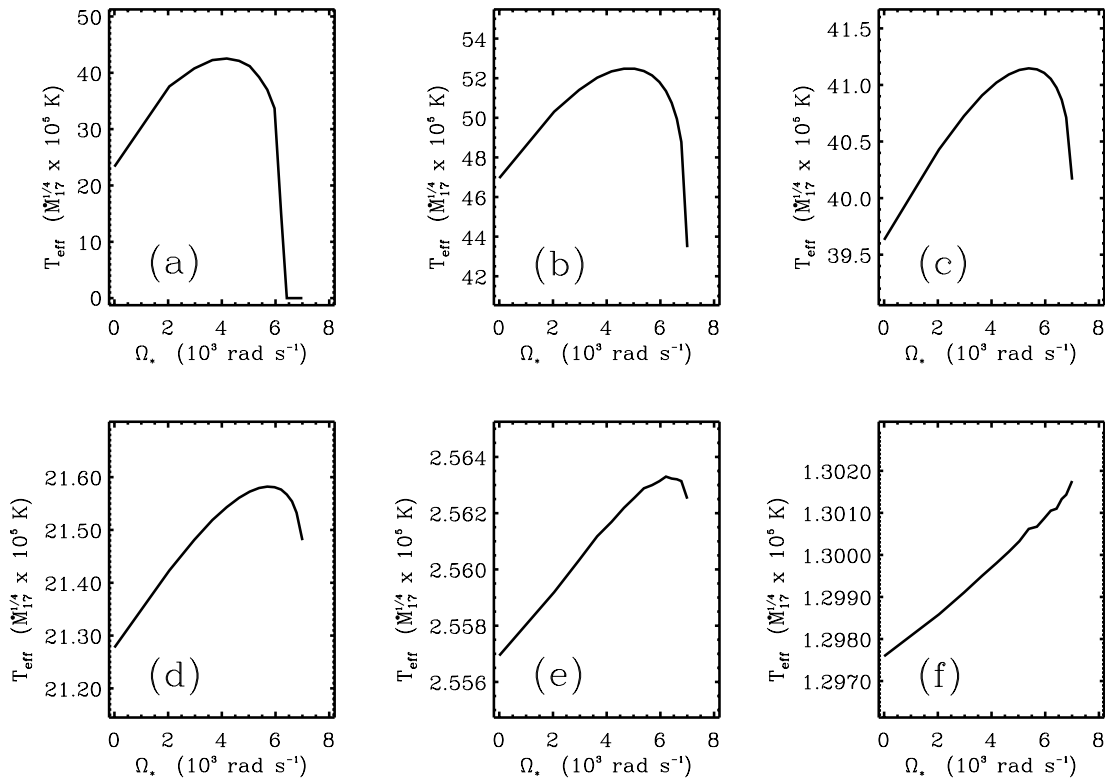
FIG. 4.—Plot of T_{eff} vs. Ω_* for chosen constant radial distances for fixed neutron star mass $M = 1.4\ M_\odot$ and EOS (B). The plots correspond to (a) $r = 13$ km, (b) $r = 18$ km, (c) $r = 35$ km, (d) $r = 100$ km, (e) $r = 2000$ km, and (f) $r = 5000$ km.
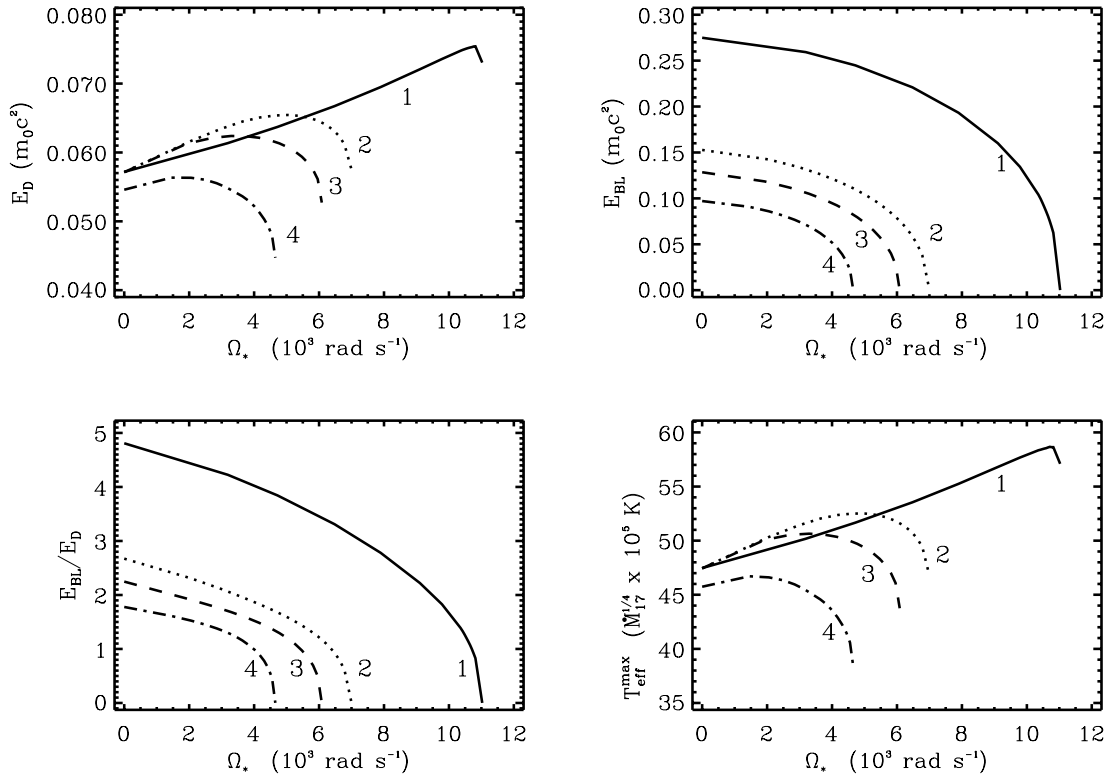
FIG. 5.—The variations of the E_D, E_{BL}, E_{BL}/E_D, and T_{eff}^{max}, with Ω_* for a chosen neutron star mass value of 1.4 $M_\odot$ for the four EOS models. The curves have the same significance as Fig. 3b.

gravitational mass corresponding to 1.4 $M_\odot$ for the EOS model B. The irradiation temperature becomes larger than the effective temperature at some large value of the radial distance, with the ratio of the former to the latter becoming increasingly large beyond this distance. For a small E_{BL} compared to E_D (as will be the case for a rapid neutron star spin rate), irradiation effects in the inner disk region will not

be significant. Defining the radial point where the irradiation temperature profile crosses the effective temperature profile as $r = r_{cross}$ and the corresponding temperature as T_{cross}, we display plots of r_{cross} and T_{cross} with Ω_* respectively in Figures 7a and 7b. It can be seen that r_{cross} increases with Ω_* just as E_D does, and hence the irradiation effect decreases with increasing Ω_*. Therefore T_{cross} decreases with increasing Ω_*.

In Figure 8 we illustrate the disk temperature (T_{disk}) profile for EOS model B corresponding to $M = 1.4$ $M_\odot$ for
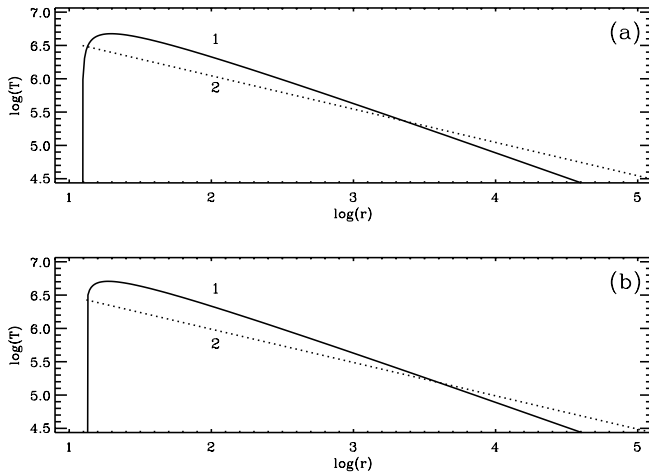
FIG. 6.—Comparison between the radial profiles of T_{eff} (curve 1) and T_{irr} (curve 2), calculated for $\eta = E_{BL} + E_D$, $\beta = 0.9$, $h/r = 0.2$, and $n = 9/7$ in eq. (10) for two values of neutron star spin rates: (a) $\Omega_* = 0$ and (b) $\Omega_* = 6.420 \times 10^3$ rad s^{-1}. The curves are for a neutron star configuration having $M = 1.4$ $M_\odot$, described by EOS model B. The temperatures are in units of $\dot{M}_{17}^{1/4}$, and the radial extent is in km. For illustrative purposes, we have displayed this comparison in a log-log plot.
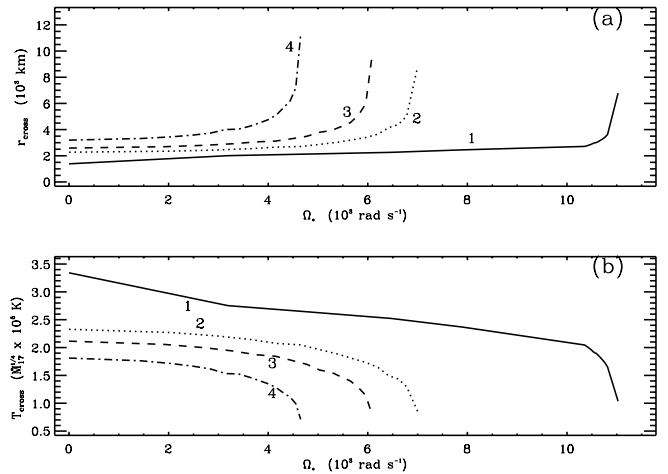
FIG. 7.—(a) r_{cross} vs. Ω_* and (b) T_{cross} vs. Ω_*. These are for a fixed neutron star gravitational mass of $M = 1.4$ $M_\odot$ and for the different EOS models as in Fig. 3b. Here T_{irr} is calculated for $\eta = E_{BL} + E_D$, $\beta = 0.9$, $h/r = 0.2$, and $n = 9/7$.
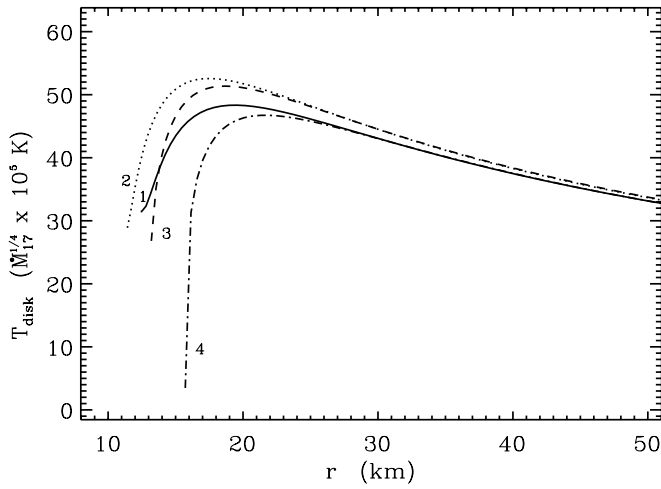
FIG. 8.—The disk temperature ($T_{\rm disk}$) profiles for a $M = 1.4$ $M_\odot$ neutron star corresponding to EOS model B, having various rotation rates as in Fig. 3a. These curves are obtained for $\eta = E_{\rm BL}$, and the same values of β, h/r, and n as in Fig. 6. are used

various values of Ω_*. In Figure 9 we illustrate the variation of $T_{\rm disk}$ with Ω_* at fixed radial points in the disk. The effect of $T_{\rm irr}$ on $T_{\rm disk}$ can be noted in Figure 9f.

4. COMPARISON WITH OBSERVATIONS: IMPLICATIONS FOR CYGNUS X-2

The X-ray spectrum will have two contributions: one from the optically thick disk and the other from the boundary layer near the neutron star surface. The spectral shape of the disk emission depends on the accretion rate. For

$\dot{M} \ll 10^{17}$ g s^{-1}, the opacity in the disk is dominated by free-free absorption and the spectrum will be a sum of blackbody spectra. The temperature of the local spectra (with respect to a comoving observer) will be equal to the temperature $T_{\rm eff}(r)$ at that radius. The observer at a large distance will see a temperature $T_{\rm obs}(r)$, which includes the effect of gravitational redshift and Doppler broadening, as mentioned in § 2. At higher accretion rates ($\dot{M} \approx 10^{17}$ g s^{-1}) the opacity will be dominated by Thomson scattering, and the spectrum from the disk is that of a modified blackbody (Shakura & Sunyaev 1973). However, for still higher accretion rates, Comptonization in the upper layer of the disk becomes important, leading to saturation in the local spectrum to form a Wien peak. The emergent spectrum can then be described as a sum of blackbody emissions but at a different temperature than $T_{\rm obs}$. The spectral temperature that is seen by a distant observer is the color temperature $T_{\rm col}$. In general, $T_{\rm col} = f(r)T_{\rm obs}$, where the function f is called the color factor (or the spectral hardening factor), and it depends on the vertical structure of the disk. Shimura & Takahara (1995) calculated the color factor for various accretion rates and masses of the accreting compact object (black hole) and found that $f \approx$ (1.8–2.0) is nearly independent of the accretion rate and the radial distance for $\dot{M} \sim \dot{M}_{\rm Edd}$. These authors find that for the accretion rate $\sim 10\%$ of the Eddington limit, $f \approx 1.7$. More recently, however, from analysis of the high-energy radiation from GRO J1655—40, a black-hole transient source observed by the Rossi X-Ray Timing Explorer (Borozdin et al. 1999) obtain a value of $f = 2.6$, which is higher than previous estimates used in the literature. With this approximation for $T_{\rm col}$, the spectrum from optically thick disks with high accretion rates can be represented as a sum of diluted blackbodies.
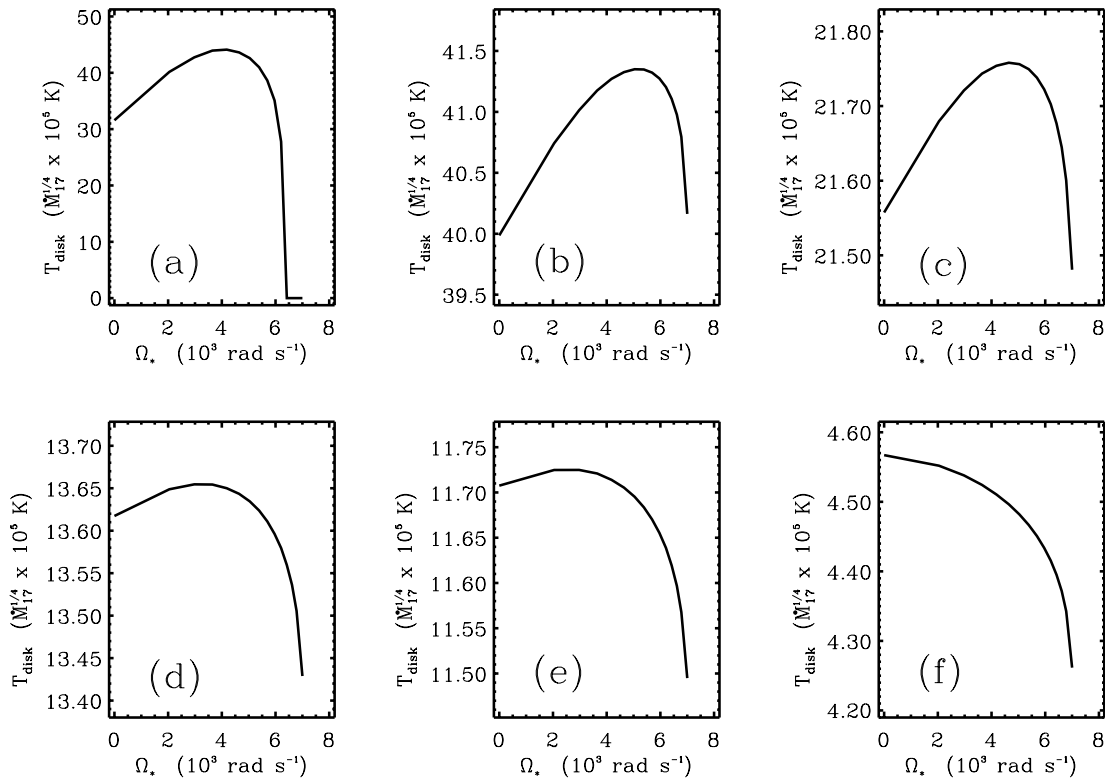
FIG. 9.—Plots of $T_{\rm disk}$ vs. Ω_* at various chosen radial distances: (a) $r = 13$ km, (b) $r = 35$ km, (c) $r = 100$ km, (d) $r = 200$ km, (e) $r = 250$ km, and (f) $r = 1000$ km. These are for EOS model B, an assumed gravitational mass value of 1.4 $M_\odot$, and the same values of η, β, h/r, and n as in Fig. 8 are used.

TABLE 2

OBSERVATIONAL CONSTRAINTS FOR EOS MODELS A, B, C, AND D

EOS	M ($M_\odot$)		f	ν_* (kHz)	ν_{in} (kHz)	R (km)	r_{eff}^{max} (km)	$\dot{M}$
A	1.4	L	1.37[1.16]	1.753[1.743]	1.755[1.755]	11.3[10.7]	16.0[15.6]	11.2[5.8]
		U	1.99[2.56]	1.755[1.755]	1.787[1.944]	11.4[11.4]	16.1[16.1]	22.9[27.5]
B	1.4	L	1.53[1.29]	1.106[1.087]	1.132[1.123]	15.2[14.3]	21.0[20.0]	13.8[7.2]
		U	2.18[2.74]	1.112[1.113]	1.177[1.285]	15.6[15.6]	21.5[21.6]	27.0[33.5]
C	1.4	L	1.57[1.33]	0.964[0.945]	0.975[0.971]	16.8[15.6]	23.1[21.7]	14.9[7.7]
		U	2.24[2.81]	0.968[0.968]	1.015[1.134]	17.2[17.2]	23.6[23.7]	29.3[36.5]
D	1.4	L	1.67[1.42]	0.736[0.719]	0.745[0.742]	20.1[18.6]	27.6[25.7]	17.5[9.1]
		U	2.38[2.97]	0.740[0.740]	0.779[0.876]	20.7[20.7]	28.3[28.4]	34.6[42.4]
B	1.78	L	1.58[1.33]	1.303[1.292]	1.322[1.315]	14.8[14.2]	21.2[20.7]	8.9[4.7]
		U	2.28[2.91]	1.307[1.307]	1.361[1.462]	15.1[15.1]	21.4[21.4]	17.2[21.4]
C	1.78	L	1.65[1.39]	1.081[1.067]	1.086[1.085]	17.1[16.2]	23.8[23.0]	9.8[5.1]
		U	2.39[3.01]	1.083[1.083]	1.109[1.209]	17.3[17.3]	24.0[24.1]	19.3[24.0]
D	1.78	L	1.74[1.47]	0.806[0.791]	0.817[0.813]	20.6[19.2]	28.6[27.1]	11.4[6.0]
		U	2.50[3.15]	0.809[0.809]	0.848[0.938]	21.1[21.1]	29.1[29.2]	22.2[27.7]

NOTE.—L and U stand for lower and upper limits. The parameters are f (color factor), ν_* (frequency of the neutron star), ν_{in} (frequency of the last orbit in the disk), R (radius of the neutron star), r_{eff}^{max} (radius where the effective temperature of the disk is maximum), and $\dot{M}$ (the accretion rate). The limits are for 25% uncertainty in luminosity and 10% uncertainty in the color temperature. Values in brackets are for 50% uncertainty in luminosity and 20% uncertainty in the color temperature. For EOS model A, the mass of the neutron star cannot exceed 1.63 $M_\odot$; hence the 1.78 $M_\odot$ solution is not presented. $\dot{M}_{Edd}$ is the Eddington accretion rate, which is $1.4 \times 10^{17} M/M_\odot$ g s^{-1}, where M is the neutron star mass.

The local flux at each radius is

$$F_\nu = \frac{1}{f^4} \pi B_\nu (fT_{eff}),$$ (12)

where B_ν is the Planck function. For high accretion rates, the boundary layer at the neutron star surface is expected to be optically thick, and an additional single-component blackbody spectrum should be observed.

The *EXOSAT* observations of Cygnus X-2 (Hasinger et al. 1986) have been fitted to several models by WSP. One of the models is of a blackbody emission up to the innermost stable circular orbit of the accretion disk and an additional blackbody spectrum to account for the boundary layer emission. The spectrum from such a disk is the sum of blackbody emission with a temperature profile

$$T \propto r^{-3/4}[1 - (r_{in}/r)^{1/2}]^{1/4} .$$ (13)

WSP have identified this temperature as the effective temperature that, as mentioned by them, is inconsistent, since the accretion rate for Cygnus X-2 is high ($\dot{M} \approx 10^{18}$ g s^{-1}). However, as mentioned above, identifying this temperature profile as the color temperature makes the model consistent if the color factor is nearly independent of radius. Moreover, the inferred temperature profile (i.e. $T_{obs} = T_{col}/f$) is similar to the one developed in the previous section. Therefore, in this paper we assume that the maximum of the best-fit color-temperature profile T_{col}^{max} is related to the maximum temperature T_{obs}^{max} computed in previous section by ($T_{col}^{max} \approx f T_{obs}^{max}$). Shimura & Takahara (1995) suggested a value of 1.85 for the factor f for an assumed neutron star mass equal to 1.4 $M_\odot$ and $\dot{M} = 10\dot{M}_{Edd}$, where $\dot{M}_{Edd}$ is the Eddington luminosity, with the mass-to-energy conversion efficiency taken as unity.

For the source Cygnus X-2, the best spectral fit to the data is when $T_{col}^{max} = 1.8 \times 10^7$ K, $L_D = 2.1 \times 10^{38}$ ergs s^{-1}, and $L_{BL} = 2.8 \times 10^{37}$ ergs s^{-1} (WSP), where L_D is the disk luminosity and L_{BL} is the luminosity in the boundary layer. The distance to the source and the inclination angle to the source have been estimated by Orosz & Kuulkers (1999) to be ≈ 8 kpc and $60°$, respectively. From these values one can

obtain, using the formalism described in § 2, the angular velocity of the neutron star (Ω_*) for a given neutron star mass, the accretion rate ($\dot{M}$), the color factor f, and the equation of state. However, in order to make an allowance for the uncertainties in the fitting procedure and in the value of z and also those arising because of the simplicity of the model, we consider a range of acceptable values for T_{col}^{max}, L_D, and L_{BL}. In particular, we allow for deviations in T_{col}^{max} and the best-fit luminosities; we take two combinations of these, namely, (10% and 25%) and (20% and 50%), where the first number in parentheses corresponds to the error in T_{col}^{max} and the second to the error in the best-fit luminosities. Note that we neglect the irradiation temperature here, since $T_{disk} \approx T_{eff}$ at the inner region of the disk (the region where the disk temperature reaches a maximum). The constraints on $\dot{M}$, Ω_*, and f are calculated for two values of the mass of the neutron star in Cygnus X-2, namely, 1.4 and 1.78 $M_\odot$. We obtain a range of consistent values for $\dot{M}$, Ω_*, and f (and, hence, allowed ranges of different quantities). The procedure is as follows:

As described in the previous section, we can calculate the different quantities (E_D, E_{BL}, T_{obs}^{max}, R, r_{in}, etc.) as a function of Ω_*. Taking the observed (or fitted) values for T_{col}^{max}, L_{BL}, and ($L_{BL} + L_D$) with the error bars, we have two limiting values for each of these quantities. We assume a particular value for each of f and $\dot{M}$, from which we obtain the corresponding fitted values of T_{obs}^{max}, E_{BL}, and ($E_{BL} + E_D$) by the relations $E_{BL} = L_{BL}/\dot{M}$, $E_{BL} + E_D = (L_{BL} + L_D)/\dot{M}$, and $T_{obs}^{max} = T_{col}^{max}/f$. By interpolation we calculate two corresponding limiting Ω_*'s (i.e., the allowed range in Ω_*) for each fitted quantity. We take the common region of these three ranges, which is the net allowed range in Ω_*. We do this for the $\dot{M}$'s in the range of 10^{-13}–10^{-6} $M_\odot$ yr^{-1} (which is reasonable for LMXB's) with a logarithmic interval of 0.0001 for a particular value of f. If, for some $\dot{M}$, there is no allowed Ω_*, then that value of $\dot{M}$ is not allowed. Thus we get the allowed range of $\dot{M}$ for a particular f. Next, we repeat the whole procedure described above for various values of f in the range of 1–10. If, for some f, there is no allowed $\dot{M}$, then that f is not allowed. Thus we get an

allowed range of f. Taking the union of all the allowed ranges of $\dot{M}$, we get the net allowed range of $\dot{M}$ (and similarly the net allowed range of Ω_*) for a particular EOS, gravitational mass, and a set of error bars. The allowed ranges of E_{BL}, E_D, R, etc. then easily follow, since their general variations with respect to Ω_* are already known. The results of this exercise for various equations of state are shown in Table 2. From Table 2 we can read off the allowed range in f, $v_* = \Omega_*/2\pi$, $v_{in} = \Omega_{K,in}/2\pi$, R, r_{eff}^{max}, and $\dot{M}$. For example, for gravitational mass $M = 1.4\ M_\odot$, with an assumed uncertainty of 25% in the luminosity and 10% uncertainty in color temperature, these are, respectively, 1.37–2.39, 0.736–1.755 kHz, 0.745–1.787 kHz, 11.3–20.7 km, 16.0–28.3 km, and 11.2–34.6 $\dot{M}_{Edd}$. On relaxing the conditions on luminosity and color temperature to 50% and 20%, respectively, the corresponding ranges change to 1.16–2.97, 0.719–1.743 kHz, 0.742–1.955 kHz, 10.7–20.7 km, 15.6–28.4 km, and 5.8–42.4 $\dot{M}_{Edd}$.

The EOS model A is the softest in the sample. The maximum mass of neutron stars (at $\Omega_* = \Omega_{ms}$) corresponding to this EOS is 1.63 $M_\odot$. Therefore the constraint results for Cygnus X-2 using this EOS are done only for $M = 1.4$ $M_\odot$. Since the luminosity in the boundary layer is about 10% of the disk luminosity, the neutron star is expected to be spinning close to the maximum allowed value. This is reflected in our results by the ratio of $\Omega_*/\Omega_{ms} \approx 0.95$. In all of these cases the neutron star radius happens to be larger than the innermost stable circular orbit. Hence the radius of the inner edge of the disk coincides with the neutron star radius. Therefore, the angular velocity of the particles in the disk inner edge will be very nearly equal to that of the neutron star. This implies that the viscous torque in the disk inner edge will not be very significant, and the use of the Page & Thorne (1974) formalism will not introduce any gross error in the constraint estimates presented by us.

5. SUMMARY AND DISCUSSION

In this paper we have calculated the temperature profiles of accretion disks around rapidly rotating and non-magnetized neutron stars using a fully general relativistic formalism. The maximum temperature and its location in the disk are found to differ substantially from their values corresponding to the Schwarzschild spacetime, depending on the rotation rate of the accreting neutron star. We have considered a model for the spectrum of the X-ray emission from the accretion disk, parameterized by the mass accretion rate, the color temperature, and the rotation rate of the star. We have compared the maximum effective temperature in the disk and the accretion luminosities (corresponding to the disk and the boundary layer) to the results of spectral fitting for the X-ray source Cygnus X-2 (WSP) and derived constraints on these parameters for the neutron star in this X-ray binary. The main conclusion of our analysis is that the neutron star in Cygnus X-2 has a rapid spin rate (close to the centrifugal mass shed value) and that the system has a fairly large accretion rate (several times 10^{18} g s^{-1}). The low luminosity of the boundary layer compared to that of the disk for Cygnus X-2 is consistent with the above conclusion that the neutron star in this system has a rapid rotation rate. The low value of the ratio L_{BL}/L_D justifies our assumption that the radiation pressure is negligible in the disk, making the geometrically thin approximation for the disk is reasonable. According to Shimura & Takahara (1995), the spectrum from the disk

can be represented as a multicolor blackbody only if $\dot{M} > 0.1\dot{M}_{Edd}$. Our results for Cygnus X-2 are in accord with this. Interestingly, if we take the lower value 1.7 for the color index f (Shimura & Takahara 1995), we obtain a consistent set of results, except for the stiffest EOS model (D). This suggests that the comparatively lower values of f would disfavor a stiff EOS for neutron star matter. However, if we take the value of $f = 2.6$, as reported by Borozdin et al. (1999), one would require an EOS model that is stiffer than the stiffest used here, or a mass greater than $M = 1.78\ M_\odot$ (if one uses the narrower limits on the luminosity and color temperature). On the other hand, if one were to use the broader limits, the hardening factor $f = 2.6$ is disallowed only by the softest EOS model.

Here we have assumed that the magnetic field of the neutron star is weak, which implies that the radius of the last orbit of the accretion disk should be much greater than the Alfvén radius r_A (e.g., Shapiro & Teukolsky 1983),

$$R \gg r_A = 2.9 \times 10^7 \left(\frac{\dot{M}}{\dot{M}_{Edd}}\right)^{-2/7} \mu_{30}^{4/7} \left(\frac{M}{M_\odot}\right)^{-3/7}, \quad (14)$$

where M is the mass of the neutron star, μ_{30} is the magnetic moment in units of 10^{30} G cm^3, and r_A is in centimeters. The above condition implies that for $R \approx 15$ km, $\dot{M}/\dot{M}_{Edd} \approx 20$, and $M = 1.4\ M_\odot$, the magnetic moment $\mu_{30} \ll 3.4 \times 10^{-2}$ or the magnetic field in the surface should be less than 10^{10} G. So the conclusions presented by us will be valid for the neutron star magnetic field up to a few times 10^9 G.

In our analysis we have assumed that the boundary layer between the disk and the neutron star surface does not affect the inner regions of the disk. This will be a valid approximation when the boundary layer luminosity is smaller than the disk luminosity and the boundary layer extent is small compared to the radius of the star. The flux received at Earth from this region is

$$F_{BL} = \left(2\pi R \frac{\Delta R}{D^2}\right) \cos\theta \left(\frac{\sigma T_{BL}^4}{\pi}\right), \quad (15)$$

where ΔR is the width of the boundary layer, $D = 8$ kpc is the distance to the source, $\theta = 60°$ is the inclination angle, and T_{BL} is the effective temperature. Spectral fitting gives a best-fit value for $F_{BL} \approx 4 \times 10^{-9}$ ergs s^{-1} cm^{-2} and $T_{BL} = T_{col(BL)}/f_{BL} = 2.88/f_{BL}$ keV, where f_{BL} is the color factor for the boundary layer and $T_{col(BL)}$ is the color temperature of the boundary layer. Using these values, $\Delta R \approx 0.2\ f_{BL}^4$ km, which is indeed smaller than R, provided the boundary layer color factor f_{BL} is close to unity. This is supported by the work of London, Taam, & Howard (1986) and Ebisuzaki (1987), who obtained $f_{BL} \approx 1.5$.

A few comments regarding the validity of the Page & Thorne (1974) formalism for accreting neutron star binaries are in order here. Unlike for the case of black holes, neutron stars possess a hard surface that could be located outside the marginally stable orbit. For neutron star binaries, this gives rise to the possibility that the disk inner edge coincides with the neutron star surface. We have assumed that the torque (and hence the flux of energy) vanishes at the disk inner edge even in cases where the latter touches the neutron star surface. In the case of rapid spin of the neutron star (as we infer for Cygnus X-2), the angular velocity of a particle in Keplerian orbit at disk inner edge will be close to the rotation rate of the neutron star. Therefore, the torque

between the neutron star surface and the inner edge of the disk is expected to be negligible. Independent of whether or not the neutron star spin is large, Page & Thorne (1974) argued that the error in the calculation of T_{eff} will not be substantial outside a radial distance r_0, where r_0 is given by $r_0 - r_{in} = 0.1\ r_{in}$. In our calculation we find that r_{eff}^{max} (which is the most important region for the generation of X-rays) is greater than r_0 by several kilometers for all the cases considered.

The shortest timescale of the system is given by the frequency in the innermost stable circular orbit (v_{in}; Table 2, col. 5). A periodic oscillation in the system should be at a frequency lower than v_{in} (unless the model invoked to explain the temporal behavior predicts substantial power in the second harmonic, i.e., $v_{QPO} \approx 2v_{in}$). The maximum frequency of the kHz QPO observed for Cygnus X-2 is 1005 Hz (Wijnands et al. 1998). The stiffest EOS, model D, will then be disfavored, since $v_{in} < 1$ kHz for this model. Further, the neutron star mass estimate in Cygnus X-2 ($\approx 1.78\ M_\odot$; Orosz & Kuulkers 1999) is not consistent with the soft EOS model A. Our analysis, therefore, favors neutron star EOS models that are intermediate in the stiffness parameters.

We have not attempted to model the observed temporal behavior of the source and, in particular, the QPO observations. Beat frequency models identify the peak separation of the two kHz QPO observed with the neutron star spin rate. For Cygnus X-2, the observed peak separation is $\Delta v = 346 \pm 29$ Hz (Wijnands et al. 1998), which is smaller than the typical rotation frequencies calculated here.

However, a pure beat-frequency model has been called into question because of several observations. For instance, Δv has been observed to vary by about 40% for Sco X-1 (van der Klis et al. 1997), and the kHz QPO frequencies have been found to be correlated with the break frequency (≈ 20 Hz) of the power spectrum density. An alternate model, where the QPOs are suggested to originate because of non-Keplerian motion of matter in the disk (Osherovich & Titarchuk 1999a, 1999b; Titarchuk & Osherovich 1999; Titarchuk et al. 1999), has been proposed. These authors have also demonstrated the model by applying it to particular sources. Inclusion of this Newtonian model into the framework of the calculations mentioned in this paper would require a parallel formulation within the spacetime geometry chosen herein.

X-ray binaries like Cygnus X-2 are believed to be the progenitors of the millisecond pulsars. Therefore, the discovery of a pulsar with a period ≈ 1 ms will strengthen the model presented in this paper in terms of a rapidly rotating accreting neutron star. X-ray spectral analysis of Cygnus X-2 and similar sources using data from recent satellites (e.g., *BeppoSAX*, *ASCA*, and the *Chandra X-ray Observatory*) is required to provide further support to the model presented in this paper.

REFERENCES

Baldo, M., Bombaci, I., & Burgio, G. F. 1997, A&A, 328, 274
Bhattacharya, D., & Datta, B. 1996, MNRAS, 282, 1059
Bhattacharya, D., & van den Heuvel, E. P. J. 1991, Phys. Rep., 203, 1
Borozdin, K., Revnivtsev, M., Trudolyubov, S., Shrader, C., & Titarchuk, L. 1999, ApJ, 517, 367
Chakrabarti, S. K., & Titarchuk, L. G. 1995, ApJ, 455, 623
Cook, G. B., Shapiro, S. L., & Teukolsky, S. A. 1994, ApJ, 424, 823
Czerny, B., Czerny, M., & Grindlay, J. E. 1986, ApJ, 311, 241
Datta, B., Thampan, A. V., & Bombaci, I. 1998, A&A, 334, 943
Datta, B., Thampan, A. V., & Wiita, P. 1995, J. Astrophys. Astron., 16, 357
Ebisuzaki, T. 1987, PASJ, 39, 287
Haberl, F., & Titarchuk, L. 1995, A&A, 299, 414
Hanawa, T. 1989, ApJ, 341, 948
Hasinger, G. Lamgmeier, A., Sztajno, M., Trümper, J., Lewin, W. H. G, & White, N. E. 1986, Nature, 319, 469
King, A. R., Kolb, U., & Burderi, L. 1996, ApJ, 464, L127
Knigge, C. 1999, MNRAS, 309, 409
Komatsu, H., Eriguchi, Y., & Hachisu, I. 1989, MNRAS, 237, 355
London, R. A., Taam, R. E., & Howard, W. M. 1986, ApJ, 306, 170
Misner, C. W., Thorne, K. S., & Wheeler, A. J. 1973, Gravitation (San Francisco: Freeman)
Mitsuda, K., et al. 1984, PASJ, 36, 741
Orosz, J. A., & Kuulkers, E. 1999, MNRAS, 305, 132

Osherovich, V. A. & Titarchuk, L. G. 1999a, ApJ, 522, L113
———. 1999b, ApJ, 523, L73
Page, D. N., & Thorne, K. S. 1974, ApJ, 191, 499
Pandharipande, V. R. 1971, Nucl. Phys. A, 178, 123
Sahu, P. K., Basu, R., & Datta, B. 1993, ApJ, 416, 267
Shakura, N. I., & Sunyaev, R. A. 1973, A&A, 24, 337
Shapiro, S. L., & Teukolsky, S. A. 1983, in Black Holes, White Dwarfs, and Neutron Stars: The Physics of Compact Objects (New York : Wiley)
Shimura, T., & Takahara, F. 1995, ApJ, 445, 780
Sunyaev, R. A., & Shakura, N. I. 1986, Soviet Astron. Lett., 12, 117
Thampan, A. V., & Datta, B. 1998, MNRAS, 297, 570
Titarchuk, L., Lapidus I., & Muslimov, A. 1998, ApJ, 499, 315
Titarchuk, L., & Osherovich, V. A. 1999, ApJ, 518, L95
Titarchuk, L., Osherovich, V. & Kuznetsov, S. 1999, ApJ, 525, L129
van der Klis, M., Wijnands, R. A. D., Horne, K., & Chen, W. 1997, ApJ, 481, L97
Vrtilek, S. D., Raymond, J. C., Garcia, M. R., Verbunt, F., Hasinger, G., & Kürster, M. 1990, A&A, 235, 162
Walecka, J. D. 1974, Ann. Phys., 83, 491
White, N. E. 1995, in X-Ray Binaries, ed. W. H. G. Lewin, J. van Paradijs, & E. P. J. van den Heuvel (Cambridge: Cambridge Univ.), 1
White, N. E., Stella, L., & Parmar, A. N. 1988, ApJ, 324, 363 (WSP)
Wijnands, R., et al. 1998, ApJ, 493, L87